

Investigating the thermally- and light-induced interconversion of bisdithiazolyl radicals and dimers with high-field EPR

Samuel M. Greer^{a,b}, Richard T. Oakley^c, Johan van Tol^a, Michael Shatruk^b, Stephen Hill^{a,d,*}

^a National High Magnetic Field Laboratory, Florida State University, Tallahassee, FL 32310, USA

^b Department of Chemistry & Biochemistry, Florida State University, Tallahassee, FL 32306, USA

^c Department of Chemistry, University of Waterloo, Waterloo, Ontario N2L 3G1, Canada

^d Department of Physics, Florida State University, Tallahassee, FL 32306, USA

ARTICLE INFO

Article history:

Received 13 April 2018

Accepted 26 June 2018

Available online 11 July 2018

Dedicated to the occasion of the 65th birthday of Professor Spyros Perlepes, in recognition of his outstanding research in coordination chemistry and molecular magnetism.

Keywords:

Photoexcitation

EPR

Radical

Dimer

Bisdithiazolyl

ABSTRACT

Materials with magnetic properties that can be modulated via optical excitation offer enticing opportunities for the development of next generation technologies. An exciting new class of photomagnetic materials based on bisdithiazolyl radicals has recently been developed. The dimorphic system in this study crystallizes in two phases, one composed of diamagnetic dimers and the other of paramagnetic radicals. Here we report on the use of high-field electron paramagnetic resonance spectroscopy to characterize both the thermally- and light-induced transitions in the dimer phase. During the course of this study we show that signals originating from residual radical defects in the dimer phase can be differentiated from those arising from the radical phase.

© 2018 Elsevier Ltd. All rights reserved.

1. Introduction

One of the biggest obstacles in the development of practical applications for photo-switchable materials is the relatively low temperature at which the photo-induced change takes place [1]. Often such materials rely on the spin crossover (SCO) phenomenon, which takes place due to a change in the electronic configuration of a transition metal-based coordination complex from a low-spin (LS) to a high-spin (HS) state [2–4]. Irradiation of the thermodynamic LS ground state allows light-induced excited-spin-state trapping (LIESST) of the metastable HS state below a characteristic temperature, T_{LIESST} , above which this metastable state decays rapidly to the LS state. In these transition metal-based systems the highest reported T_{LIESST} is 180 K [5]. With the current record being well below room temperature, practical applications of such materials remain problematic. Ideally one would like to develop a material capable of exhibiting the photo-induced switching at room temperature.

Light-induced radical trapping (LIRT) [6], an effect analogous to LIESST, has recently been observed in organic materials where the change in spin state is due to the dimerization of a pair of π -radicals into a diamagnetic σ -dimer [6–8]. This radical \rightarrow dimer transition is conceptually similar to the HS \rightarrow LS transition observed in 3d metal-based SCO complexes. In the solid state, the diamagnetic dimer can be split into a metastable pair of radicals via photo-excitation at low temperatures. The T_{LIRT} (analogous to T_{LIESST}) of the bisdithiazolyl species studied here has previously been determined to be 242 K, significantly higher than the T_{LIESST} values typically observed in transition metal systems [1]. This compound was found to crystallize in two distinct polymorphs, **1 α** and **1 β** , with room temperature $\chi^{\prime\prime}T$ products indicative of paramagnetic $S = 1/2$ and diamagnetic $S = 0$ phases, respectively. The **1 β** polymorph undergoes a thermally induced hysteretic phase transition resulting in the formation of a pair of radicals above 380 K and the recovery of a diamagnetic hypervalent σ -bonded dimer below 375 K (Fig. 1). At temperatures below 242 K, irradiation of the sample cleaves the hypervalent 4-center 6-electron $S \cdots S - S \cdots S$ bond, generating two stable π -radicals. Few studies characterizing the photogeneration of a metastable paramagnetic state have been performed on radical-based systems. The persistent nature of these

* Corresponding author at: National High Magnetic Field Laboratory, Florida State University, Tallahassee, FL 32310, USA.

E-mail address: shill@magnet.fsu.edu (S. Hill).

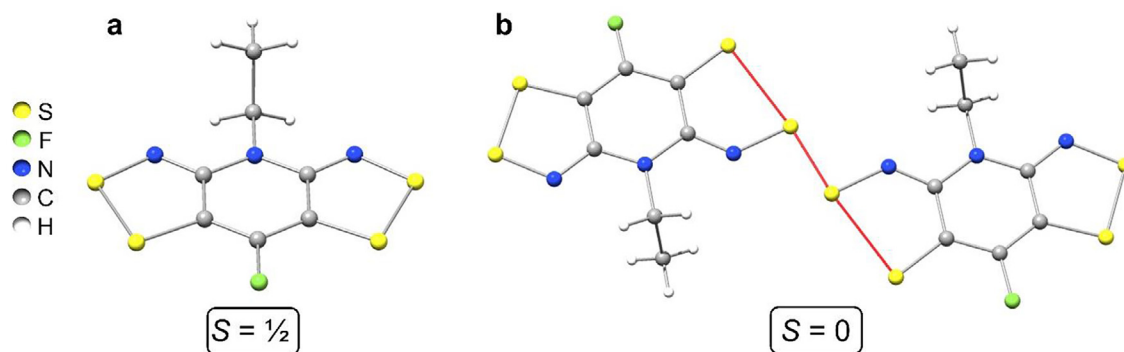


Fig. 1. Molecular structures of the bisdithiazolyl π -radical (a) and the σ -dimer (b). The red bonds in the σ -dimer highlight the 4 center – 6 electron hypervalent interaction. (Color online.)

photoinduced states makes them conceptually different from transient triplet states generated in traditional organic photochemistry [9,10]. To investigate this novel phenomenon, we have performed a series of high-field electron paramagnetic resonance (HF-EPR) experiments probing both the thermal- and light-induced transitions.

2. Materials and methods

2.1. Synthesis

Compounds **1 α** and **1 β** were synthesized as previously reported [7].

2.2. High-field electron paramagnetic resonance (homodyne detection)

Experiments on **1 α** were performed on a microcrystalline powder sample which was immobilized in a polyethylene cup using a Teflon[®] stopper. The transmission-type spectrometer employed a phase locked Virginia Diodes source combined with a series of frequency multipliers to generate the various microwave frequencies. The field modulated signal was detected using a hot electron InSb bolometer. Temperature control was achieved using an Oxford Instruments continuous-flow cryostat housed in a 15/17 T superconducting Oxford Instruments magnet [11].

2.3. High-field electron paramagnetic resonance (heterodyne detection)

Photo-excitation experiments on **1 β** were performed on a microcrystalline powder sample dispersed in mineral oil and contained in a transparent polyethylene cup. Light irradiation was performed through an optical window in the probe using a NiteRider MiNewt 600 cordless rechargeable headlight capable of producing 600 Lumens of light output. Dispersion of the sample in mineral oil was necessary to ensure light transmission through the entire sample and to maximize the number of crystallites exposed to the light. To facilitate collection of the high temperature spectra, a second sample was prepared in a polyether ether ketone (PEEK, melting point \sim 616 K) container and sealed with a tightly fitted PEEK stopper. This spectrometer utilizes a super-heterodyne quasi-optical bridge in conjunction with 12.5 T Oxford Instruments superconducting magnet [12,13].

2.4. EPR spectral simulations

All spectral simulations were performed using the program EasySpin [14].

3. Results and discussion

All EPR spectra were analyzed in the framework of a standard Zeeman spin Hamiltonian:

$$\hat{H}_{spin} = \beta_e \vec{B} \cdot \vec{g} \cdot \hat{S} \quad (1)$$

where β_e is the Bohr magneton, \vec{B} is the applied magnetic field vector, \vec{g} is the Landé g -tensor, and \hat{S} is the total spin operator [15]; no zero-field splitting (ZFS) or hyperfine interactions were detectable for either **1 α** or **1 β** .

3.1. High-field EPR of **1 α**

The room temperature EPR signal of **1 α** exhibits a linear frequency dependence with respect to the applied field, extrapolating to zero frequency at zero field (Fig. 2). This behavior is indicative of a Kramers doublet ground state where the lack of a measurable frequency-independent ZFS term suggests that intermolecular coupling is weak [16]. Simulations of the spectra result in $g_{x,y} = 2.0099(8)$ and $g_z = 2.0042(8)$. However, variable temperature measurements performed at 304.8 GHz reveal the presence of intermolecular interactions through an increase in the observed spectral linewidth at the lowest temperatures (Fig. 2). In spite of this, the g -anisotropy observed at room temperature is still resolvable at the lowest temperatures. These findings are consistent with previous magnetic measurements which show that, above \sim 20 K, the system behaves as a Curie–Weiss paramagnet and, below this temperature, it can be modelled as a Heisenberg chain of weakly antiferromagnetically coupled radicals [7].

3.2. High-field and high temperature EPR of **1 β**

As described in the introduction, **1 β** exists as a diamagnetic σ -dimer upon cooling below \sim 375 K. We have thus recorded variable temperature EPR spectra between 290 and 385 K (Fig. 3). The 290 K spectrum shows two prominent features, one at $g \sim$ 2.010 and the other at around $g \sim$ 2.008. With increasing temperature, the lower-field feature decreases in intensity while the higher-field one exhibits a sharp increase in intensity at \sim 375 K. The g -value of the feature with decreasing intensity is identical to that of the $g_{x,y}$ component of **1 α** , suggesting that it may be attributed to a small amount of **1 α** contaminant in the powder. Meanwhile, below 375 K, the higher field signal can be assigned to non-dimerized radical defects occurring in the dimer phase of **1 β** . In order to relate the intensity of the EPR spectrum to the radical population, we evaluate the double integral of the recorded dI/dB spectrum at each temperature, which is proportional to the spin susceptibility, χ' . We then plot the $\chi'T$ product versus temperature (Fig. 3, inset) in order to correct for the $1/T$ Boltzmann dependence of the spectral

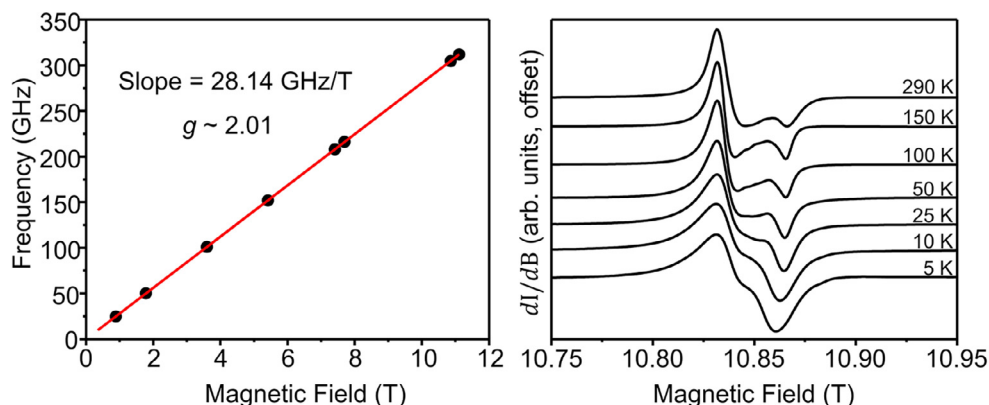


Fig. 2. (left) Frequency dependent resonance position for **1α** at room temperature. (right) Variable temperature EPR spectra of **1α** recorded at 304.8 GHz in field derivative mode, dI/dB , where I represents the microwave signal intensity reaching the detector.

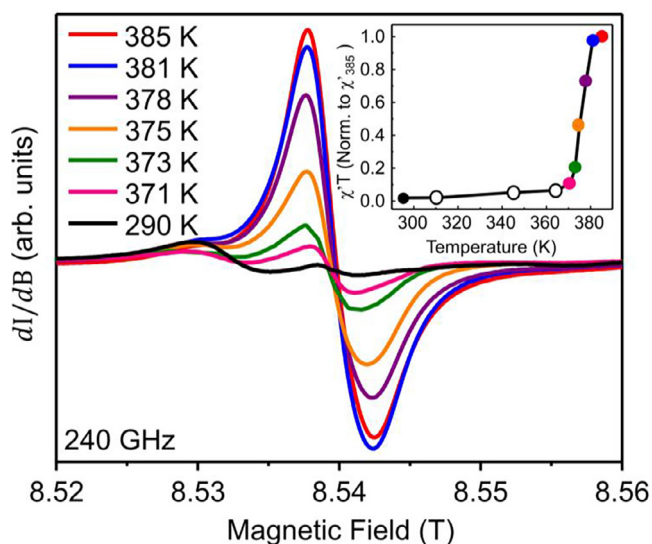


Fig. 3. Variable temperature EPR spectra of **1β** recorded at 240 GHz demonstrating the conversion from the diamagnetic σ -dimers to paramagnetic π -radicals due to thermally induced bond cleavage. The inset shows the product of the doubly integrated dI/dB signal ($\equiv \chi'$) and temperature, normalized to the 385 K product; the same colors are used in the inset and the main panel, with hollow data points for spectra that are not shown. Double integration is required because of the use of field modulation in the experiment, which transforms the EPR intensity (I) into a first derivative signal (dI/dB).

intensity. The $\chi'T$ product, therefore, provides a direct measure of the radical concentration in the sample, and its abrupt rise in the 370–380 K range confirms the expected spin transition and the accompanying sharp increase in radical concentration due to thermal cleaving of the hypervalent bond in the dimer. Interestingly, even below 375 K, a slow increase in the $\chi'T$ product with temperature is observed, suggesting a gradual increase in radical defects in the dimer phase of **1β**. It has been shown that such defects can occur in the bulk material with minimal changes to the crystal structure [17]. By comparing to the fully cleaved 385 K $\chi'T$ product, we estimate that $\sim 2\%$ of the bisdithiazolyl molecules remain in the π -radical (non-dimerized) form at room temperature.

3.3. High field EPR of **1β** under light irradiation

At 100 K, **1β** exists as a diamagnetic σ -dimer. However, upon photoexcitation, it converts into a pair of stable π radicals. Fig. 4a shows the 100 K/240 GHz spectrum before and after white light irradiation. Similar to the temperature dependent spectra, we observe one feature with intensity independent of light exposure (**1α** impurity at ~ 8.53 T) and two features with strong responses characterized by $g_x = g_y = 2.0085(5)$ and $g_z = 2.0066(5)$. Temperature dependent studies of the photo-generated state show that the spectrum returns to its original form at room temperature, thus demonstrating the reversibility of the LIRT effect.

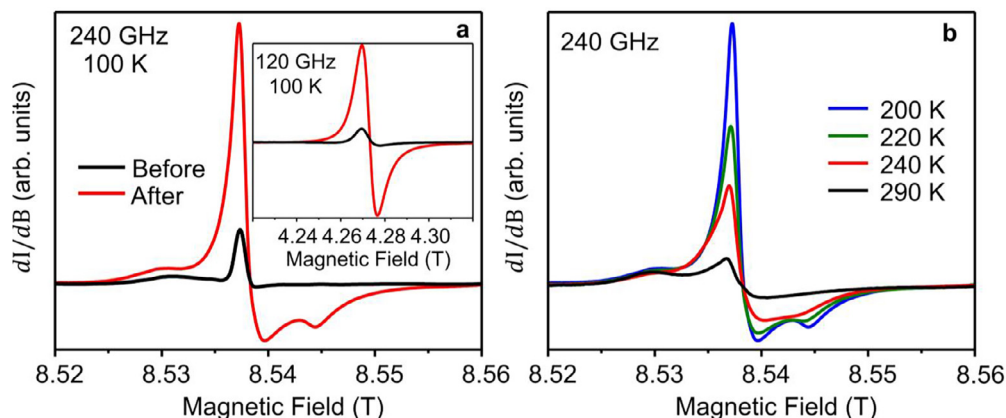


Fig. 4. (a) Effect of white light irradiation on a powder sample of **1β** at 100 K, recorded at 240 GHz. The black and red traces show the signal before and after light irradiation, respectively. The inset shows the 120 GHz, 100 K spectrum of a single crystal of **1β** before and after light exposure. The rod-shaped crystal was oriented with the long side perpendicular to the applied magnetic field. (b) Temperature dependence of the EPR signal for the photo-generated species.

Table 1
Spin Hamiltonian parameters[^] used to simulate the HF EPR data.

	T (K)	g_x	g_y	g_z	g_{avg}	Space group
1α	100	2.0099(8)	2.0099(8)	2.0042(8)	2.0080	$P4_2/m$
1β^{Therm}	385	2.0082(5)	2.0082(5)	2.0072(5)	2.0079	$P2_1/c$
1β^{LIRT}	100	2.0085(5)	2.0085(5)	2.0066(5)	2.0079	$P2_1/c$

[^] The numbers in parentheses indicate the estimated uncertainty of the last digit.

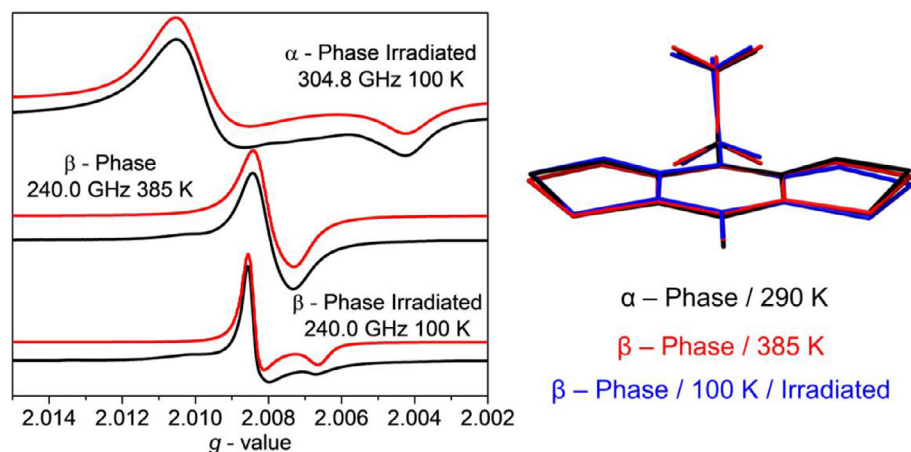


Fig. 5. (left) Representative experimental spectra (black traces) and simulations (red traces) of **1 α** (5.1 mT Lorentzian linewidth), thermally cleaved **1 β^{Therm}** (2.7 mT Lorentzian linewidth), and light irradiated **1 β^{LIRT}** (1.2 mT Lorentzian linewidth), under the indicated conditions. (right) Overlay of the crystal structures showing the minute differences under various conditions: **1 α** at 290 K (black); **1 β^{Therm}** at 393 K (red); and light irradiated **1 β^{LIRT}** at 100 K (blue).¹ (Color online.)

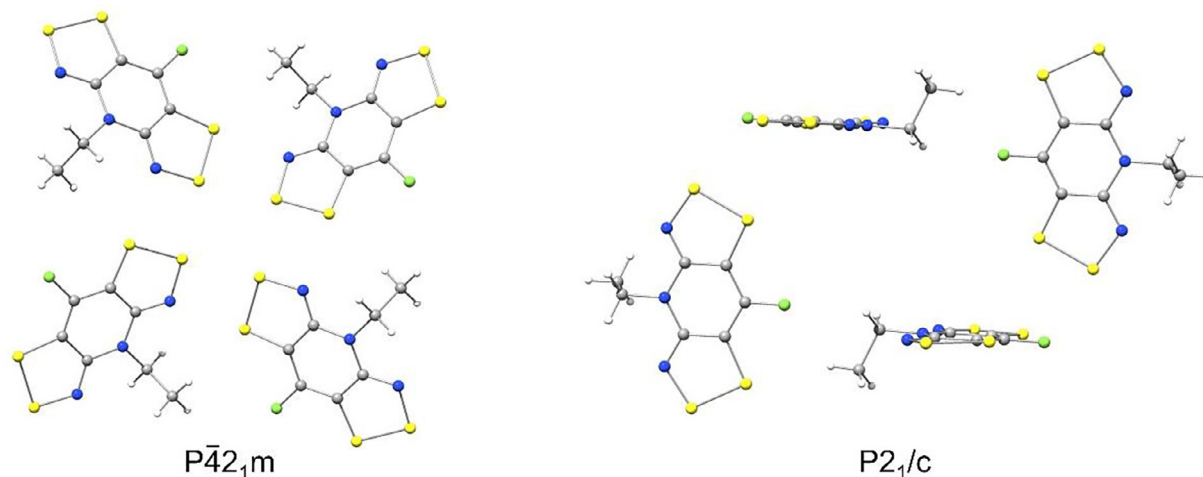


Fig. 6. Crystal packing of **1 α** (left) and the π -radical form of **1 β** (right) in the $P4_2/m$ and $P2_1/c$ space groups, respectively.

3.4. Spectroscopic and structural comparisons of **1 α** , high temperature **1 β^{Therm}** , and irradiated **1 β^{LIRT}**

Representative spectra along with their corresponding simulations, generated using the parameters in Table 1, are shown in Fig. 5. The sizable changes in g -factors observed between **1 α** and **1 $\beta^{Therm/LIRT}$** are somewhat unexpected. A direct comparison of the molecular structures reveals only minor geometric differences, suggesting that packing interactions may be responsible for the differences.¹ This is supported by the different crystallographic space groups of each phase (Fig. 6): **1 α** crystallizes in the tetragonal space group $P4_2/m$, where four columns of π -stacked radicals conform to

a fourfold rotation around the c -axis; **1 β** crystallizes in the $P2_1/c$ space group in which the π stacking is disrupted, as two of the molecules in the unit cell are rotated by $\sim 90^\circ$ from the others. The cause of the variations in g -values between the thermal- and photo-generated species is more subtle and likely results from the expansion of the lattice with increasing temperature which alters the exchange interaction pathways and, in turn, the g -values [18].

In all recorded spectra of **1 β** below 345 K, and without light excitation, we observe a feature (visible at ~ 8.538 T in the 290 K spectra in Figs. 3 and 4) with a g -value that is similar to the g_x/g_y values of both the **1 β^{Therm}** and **1 β^{LIRT}** species (~ 2.0085). We propose that this residual radical signal, as well as the ‘Curie tail’ observed in the magnetic data [7], results from non-dimerized radical defects in the dimer phase. These radical defects are different from those produced by the LIRT mechanism and the thermally induced transition. Based on the spectral signature of this defect, it

¹ The structural model used in the solution of the powder x-ray diffraction data was only partially refined. For details see Ref. [6].

is likely to reside in a lattice environment only slightly different from that of the photo- and thermally-generated radicals [19]. In contrast to the bulk material, however, these sites are unable to link with neighboring sites during dimer formation, most likely due to the loss of structural coherence, i.e., there is a break in radical proximity. To support this claim, we have studied a single crystal of 1β which indeed shows a single feature that increases in intensity upon irradiation (Inset of Fig. 4a), and no contamination due to 1α . While these defects are visible in the EPR data they are not sufficiently high in concentration to be observed crystallographically and, based on the analysis of the EPR spectral weight monitoring the thermally induced transition, make up only $\sim 2\%$ of the bulk material.

4. Conclusions

In summary, we have performed a series of high-field EPR measurements on two polymorphs of a magnetically photo-switchable bisdithiazolyl compound. At high-frequencies and high-fields, the two crystallographic phases are shown to be easily distinguishable based on their g -tensors. We note that this would not have been possible at low-fields/frequencies due to decreased spectral resolution. Through variable temperature measurements we have determined that radical defects make up $\sim 2\%$ of the 1β dimer phase and are observed at all temperatures below ~ 380 K. Furthermore, we have shown that these defects cannot be explained as impurities of 1α . As more examples of these switchable radical/dimer systems are characterized, this behavior may prove to be common.

Acknowledgements

A portion of this work was performed at the National High Magnetic Field Laboratory (NHMFL), which is supported by the National Science Foundation (Cooperative Agreements DMR-1157490 and DMR-1644779) and the State of Florida. SMG acknowledges support from the National Science Foundation Graduate Research Fellowship Program (DGE-1449440). Support from the Natural Sciences and Engineering Council of Canada (NSERC to RTO) and the National Science Foundation (DMR-1610226 to SH and CHE-1464955 to MS) is also acknowledged.

References

- [1] J.-F. Létard, L. Capes, G. Chastanet, N. Moliner, S. Létard, J.-A. Real, O. Kahn, Critical temperature of the LIESST effect in iron(II) spin crossover compounds, *Chem. Phys. Lett.* 313 (1999) 115–120, [https://doi.org/10.1016/S0009-2614\(99\)01036-2](https://doi.org/10.1016/S0009-2614(99)01036-2).
- [2] M.A. Halcrow, *Spin-Crossover Materials: Properties and Applications*, Wiley-Blackwell, 2013.
- [3] P. Gütllich, H.A. Goodwin, in: *Spin Crossover in Transition Metal Compounds II*, Springer, Berlin, Heidelberg, 2004, <https://doi.org/10.1007/b93641>.
- [4] A. Bousseksou, G. Molnár, L. Salmon, W. Nicolazzi, Molecular spin crossover phenomenon: recent achievements and prospects, *Chem. Soc. Rev.* 40 (2011) 3313, <https://doi.org/10.1039/c1cs15042a>.
- [5] D. Li, R. Clérac, O. Roubeau, E. Harté, C. Mathonière, R. Le Bris, S.M. Holmes, Magnetic and optical bistability driven by thermally and photoinduced intramolecular electron transfer in a molecular cobalt-iron Prussian blue analogue, *J. Am. Chem. Soc.* 130 (2008) 252–258, <https://doi.org/10.1021/ja0757632>.
- [6] H. Phan, K. Lekin, S.M. Winter, R.T. Oakley, M. Shatruk, Photoinduced solid state conversion of a radical σ -dimer to a π -radical pair, *J. Am. Chem. Soc.* 135 (2013) 15674–15677, <https://doi.org/10.1021/ja4055806>.
- [7] K. Lekin, S.M. Winter, L.E. Downie, X. Bao, J.S. Tse, S. Desgreniers, R.A. Secco, P. A. Dube, R.T. Oakley, Hysteretic spin crossover between a bisdithiazolyl radical and its hypervalent σ -dimer, *J. Am. Chem. Soc.* 132 (2010) 16212–16224, <https://doi.org/10.1021/ja106768z>.
- [8] K. Lekin, H. Phan, S.M. Winter, J.W.L. Wong, A.A. Leitch, D. Laniel, W. Yong, R.A. Secco, J.S. Tse, S. Desgreniers, P.A. Dube, M. Shatruk, R.T. Oakley, Heat, pressure and light-induced interconversion of bisdithiazolyl radicals and dimers, *J. Am. Chem. Soc.* 136 (2014) 8050–8062, <https://doi.org/10.1021/ja502753t>.
- [9] J. van Tol, L.C. Brunel, A. Angerhofer, Transient EPR at 240 GHz of the excited triplet state of free-base tetra-phenyl porphyrin, *Appl. Magn. Reson.* 21 (2001) 335–340, <https://doi.org/10.1007/BF03162412>.
- [10] C.E. Tait, P. Neuhaus, M.D. Peeks, H.L. Anderson, C.R. Timmel, Transient EPR reveals triplet state delocalization in a series of cyclic and linear π -conjugated porphyrin oligomers, *J. Am. Chem. Soc.* 137 (2015) 8284–8293, <https://doi.org/10.1021/jacs.5b04511>.
- [11] A. Hassan, L. Pardi, J. Krzystek, A. Sienkiewicz, P. Goy, M. Rohrer, L.-C. Brunel, Ultrawide band multifrequency high-field EMR technique: a methodology for increasing spectroscopic information, *J. Magn. Reson.* 142 (2000) 300–312, <https://doi.org/10.1006/jmre.1999.1952>.
- [12] G.W. Morley, L.-C. Brunel, J. van Tol, A multifrequency high-field pulsed electron paramagnetic resonance/electron-nuclear double resonance spectrometer, *Rev. Sci. Instrum.* 79 (2008) 64703, <https://doi.org/10.1063/1.2937630>.
- [13] J. van Tol, L.-C. Brunel, R.J. Wylde, A quasi-optical transient electron spin resonance spectrometer operating at 120 and 240 GHz, *Rev. Sci. Instrum.* 76 (2005) 74101, <https://doi.org/10.1063/1.1942533>.
- [14] S. Stoll, A. Schweiger, EasySpin, a comprehensive software package for spectral simulation and analysis in EPR, *J. Magn. Reson.* 178 (2006) 42–55, <https://doi.org/10.1016/j.jmr.2005.08.013>.
- [15] A. Abragam, B. Bleaney, *Electron Paramagnetic Resonance of Transition Ions*, Oxford University Press, 2012.
- [16] F.E. Mabbs, D. Collison, *Electron Paramagnetic Resonance of d Transition Metal Compounds*, Elsevier Science, Amsterdam, 1992.
- [17] V.I. Nikolayenko, L.J. Barbour, A. Arauzo, J. Campo, J.M. Rawson, D.A. Haynes, Inclusion of a dithiadiazolyl radical in a seemingly non-porous solid, *Chem. Commun.* 53 (2017) 11310–11313, <https://doi.org/10.1039/C7CC06678C>.
- [18] S.L. Veber, M.V. Fedin, A.I. Potapov, K.Y. Maryunina, G.V. Romanenko, R.Z. Sagdeev, V.I. Ovcharenko, D. Goldfarb, E.G. Bagryanskaya, High-field EPR reveals the strongly temperature-dependent exchange interaction in “breathing” crystals Cu(hfac)₂LR, *J. Am. Chem. Soc.* 130 (2008) 2444–2445, <https://doi.org/10.1021/ja710773u>.
- [19] S. Stoll, High-field EPR of bioorganic radicals, *Electron Paramagn. Reson.*, 2010, pp. 107–154, <https://doi.org/10.1039/9781849730877-00107>.